Unraveling the Nature of Lasing Emission from Hybrid Silicon Nitride and Colloidal Nanocrystal Low Refractive Index Photonic Crystals

I. Tanghe[1,2,3], T. Vandekerckhove[1], M. Samoli[2], A. Waters,[4] D. Harankahage[5,6], M. Zamkov,[4,6] Z. Hens[2], C. Seassal[7], H-S Nguyen[7], D. Van Thourhout,[1] and P. Geiregat[2,3].

[1] Photonics Research Group, Ghent University, Belgium
[2] Physics and Chemistry of Nanostructures, Ghent University, Belgium
[3] NoLIMITS Center for Non-Linear Microscopy and Spectroscopy, Ghent University, Belgium
[4] Department of Physics, Bowling Green State University, Bowling Green, Ohio, USA
[5] Department of Chemistry, Bowling Green State University, Bowling Green, Ohio 43403, USA
[6] The Center of Photochemical Sciences, Bowling Green State University, Bowling Green, Ohio, USA
[7] Institut des Nanotechnologies de Lyon, Universite de Lyon, Centre National de la Recherche Scientifique, Ecole Centrale de Lyon, Ecully, France

Silicon nitride is used for its low optical loss and high thermal stability, making it a suitable platform for visible-light applications within integrated photonic devices. However, its application has been limited due to inefficient light emission, a problem addressed by integrating various types of light emitters onto the platform through heterogeneous integration. In particular, the integration of solution-processable colloidal nanocrystals (NCs) as optical gain materials onto the silicon nitride platform is a promising route, but requires a more solid theoretical footing. Recently, demonstrations of lasing employing CdS bulk nanocrystals and CdSe/CdS Quantum Shells using 2D surface emitting photonic crystal structures have shown exciting results[1,2] of lasing from green to red. Building on this, we model the light-matter interactions of the low index contrast NC/nitride platform for thorough understanding. This modeling shows the clustering of all the optical modes within a spectrally narrow bandwidth.

Introduction

The drive towards miniaturization in photonics implicates a need for compact, efficient, on-chip lasers capable of precise wavelength selectivity and directional emission. These devices are crucial across a variety of applications, including micro-displays, tunable light sources, and advanced sensing/imaging systems. The need for integrating multiple laser sources on a single chip, without compromising performance, poses significant challenges in terms of possible device architectures and commensurate compatibility of the active materials.

Silicon photonics has emerged as a robust platform for addressing these challenges, particularly through the use of silicon nitride (SiNx), which offers excellent properties for visible-light applications due to its low optical loss in this part of the spectrum, and a high thermal stability. By now, losses as low as 1 dB/m are achievable, allowing for quality factors (Q) above 1 million.[1] SiNx's compatibility with standard CMOS fabrication processes further enhances its appeal for integrated photonic devices. However, despite its potential as a passive platform, the lack of efficient light emission from SiNx limits its wider application.

In this context, the integration of solution processable colloidal nanocrystals (NCs) onto SiNx presents a transformative approach for achieving the desired enhanced functionality. Indeed, NCs are obtained as an ink and hence are processable from a solution phase allowing for cost-effective and straightforward methods for integration onto photonic chips, such as spin coating, Langmuir-Blodgett deposition and/or inkjet printing. Using their broadband and size-tunable absorption, efficient optical gain metrics have been demonstrated, [2,3,4] which is critical for the development of the highly desired

on-chip laser sources mentioned above. Several demonstrations in literature indicated the potential for lasing on the nitride platform, both in the green and red part of the visible spectrum under quasi-CW optical excitation.[3,4] Also electrically excited amplified spontaneous emission (ASE) sources have been demonstrated.[5,6] In these demonstrations, a recent trend towards photonic crystal cavities can been observed – both with one- and two-dimensional confinement – due to the ease of processing, as they consist of a single lithography step followed by depositing the active NC layer on top. These photonic crystal surface emitting lasers (PCSEL) implementations benefit from efficient collection of the collimated out-of-plane emission combined with efficient in-plane feedback, allowing for quick demonstrations of lasing in proof-of-concept experiments across the visible and near-infrared spectrum.[3,4,7] While Photonic Crystal (PhC) - based laser structures combined with NCs have been presented in the past, they are typically not explored in-depth from a purely photonic perspective and more used as a means to an end.

In this work, we first demonstrate and characterize lasing from SiNx PhC devices coated with thin layers of NCs, thereby using two state-of-art colloidal gain materials: red-emitting CdSe/CdS quantum shells (QSs)[4] and green-emitting CdS bulk nanocrystals (BNCs)[3]. Both materials were spin coated from a colloidal dispersion on similar SiNx chips, underscoring the versatility of the hybridization approach. Next, we take one step back and develop the theory behind these hybrid devices by simulating the photonic band structures of the low refractive index contrast SiNx/NC systems using the Finite Element Method (FEM). The simulations allow to identify and catalog the various possible modes and their energy dispersion.[8]

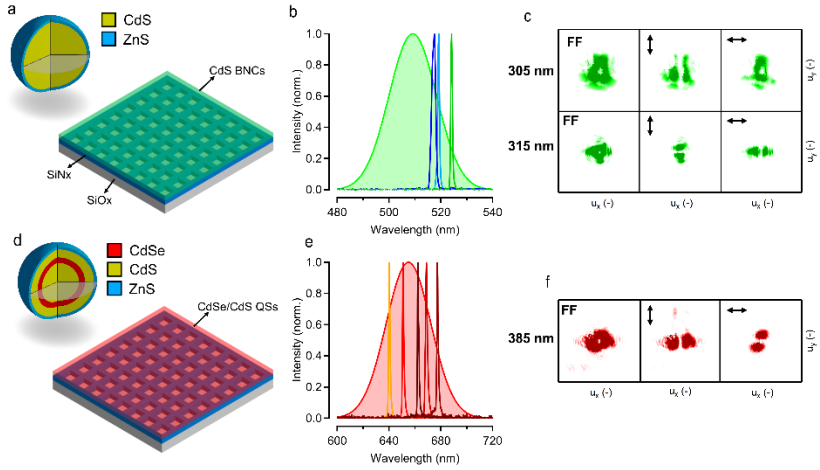

Figure 1: Lasing characteristics of hybrid colloidal nanocrystal/silicon nitride 2D photonic crystal structures. (top) using CdS Bulk Nanocrystals. (bottom) using CdSe/CdS Quantum Shells.

Lasing from Colloidal NC/SiNx 2D PhC Devices

PhC devices are fabricated on a SiNx-on-SiOx platform, where periodically etched holes with a designed 60% duty cycle are etched into a 170 nm thick SiNx layer with periods ranging from 300 to 425 nm, in increments of 5 nm, designed to tune the photonic band structure, where increasing the period will red-shift the bands. Following the etching process, NCs are spin-coated from solution onto the devices under ambient conditions. This typically fills the etched holes and forms an overcoat of approximately 50 nm thick.

In this work, we prepared three distinct chip variants with a relevant period sweep for experimental analysis: a bare structure without NCs, one incorporating CdS BNC[3] (Figure 1a-c), and another with CdSe/CdS QSs[4] (Figure 1d-f). The periods range from 300 - 380 nm for the bare SiNx chip, 300 - 340 nm for the BNC/SiNx chip and 385 - 425 nm for the QS/SiNx chip. Figures 1a and d show schematics of a device emitting green and red light, respectively, and the insets depict a schematic of the NC material's core/shell architecture. The photoluminescence (PL) and lasing peaks for these materials are illustrated in Figures 1b and e. For the green chip, PL ranges from 490 to 530 nm, with lasing observed between 515 and 525 nm. The green-emitting colloidal NCs used here are CdS NCs with a diameter around 12 nm, larger than the Bohr-radius. As such, they behave optically like bulk CdS, as studied before[3] The red chip shows PL from 620 to 690 nm, with a lasing range of 640 to 680 nm. The red-emitting colloidal NCs are large CdS core QSs, where the carriers are mainly confined within the first shell of CdSe.[4] Their total diameter is about 21 nm. The observed spectral bandwidth over which lasing is obtained is in line with previous reports, beit slightly narrower due to the more restricted PhC lattice period sweep used in this study.

Additionally, Figures 1c and 1f include an analysis of the polarized and unpolarized far-field patterns for multiple devices, which are crucial for assessing the specific optical mode that is resonating. All patterns exhibit a typical ring-shaped far-field pattern for these types of structures. For the green-emitting devices, both smaller periods (300 and 305 nm) exhibit the same far-field patterns, shown in Figure 1c (top), with two horizontal (vertical) lobes when vertically (horizontally) polarized. The device with the larger period (315 nm) however displays the inverse: horizontal (vertical) lobes when horizontally (vertically) polarized, as shown at the bottom of the same figure. The red-emitting devices consistently show similar far-field patterns across all devices that exhibit lasing, as depicted in Figure 1f. The same ring-shaped far-field pattern is seen, where the polarized measurements display similar behavior as the shorter period green devices.

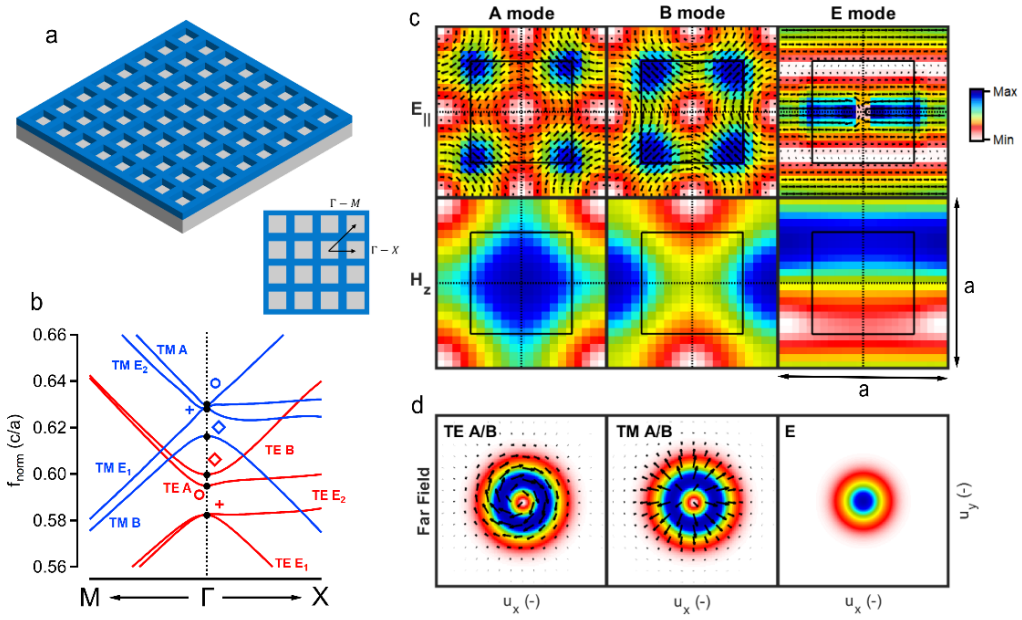

Figure 2: Photonic Band Structure, Mode Profiles at the Γ-point, and far field patterns.

Modeling 2D PhC Band Structures and Optical Modes

In this study, we investigate devices characterized by square-like periodicity across two dimensions, as shown in Figure 2a. Light is confined within these two dimensions (in-plane) and only confined due to index contrast in the third dimension, which is perpendicular (out-of-plane). Typically, such devices are described through second order Bragg diffraction, described by the equation $m \cdot \lambda = 2n_{eff} \cdot \Lambda$, where $m = 2$ corresponds to second-order diffraction. This configuration allows for both perpendicular (out-of-plane, 90˚) and backward (in-plane, 180˚) scattering. The combination of both in-plane and out-of-plane scattering is crucial for device operation: in-plane is necessary for confinement, whereas out-of-plane enables surface emission.

By solving Maxwell's equations for these devices using finite element modeling (FEM), we find eight possible optical (eigen)modes, each with a distinct polarization and spatial symmetry. These modes' field profiles can be catalogued into two groups: Transverse Electric (TE) modes, which have only in-plane electric field components and an out-of-plane magnetic field component, and Transverse Magnetic (TM) modes, where the field distributions between electric and magnetic components are swapped compared to TE. The presence of these modes at distinct wavelengths stems from their different field profiles present in each material of the device, known as geometric dispersion.

The modes are also categorized based on the symmetry of their out-of-plane components.[8] With square-like symmetry, this system belongs to the C_4 point group, and therefore so will the optical modes that are the solutions. The mode invariant under all symmetry operations is labelled as the *A*-mode. The mode that inverts under 90˚ or 270˚ rotations and remains constant for the other operations is the *B*-mode. The other two modes, E_1 and E_2, are degenerate and span a space where symmetry operations transform their field distributions into linear combinations of both. Both the TE and TM modes share this out-of-plane field distribution, except that *E*- and *H*-fields are swapped. This symmetry-centric approach provides a comprehensive understanding of the optical behaviour within these structured fields. The various field profiles for a single period are displayed in Figure 2c, specifically for the TE modes. Only one of the *E*-modes is displayed, the other solution is the same yet rotated over 90˚.

The symmetry of the optical mode heavily influences the emission properties of the structure. For the *A*- and *B*-mode the in-plane fields are anti-symmetric with respect to the *x*- and *y*-axes, leading to destructive interference for upward scattered light. This interference nullifies the amplitude of this component, effectively confining the light completely within the plane. This phenomenon is crucial for the high quality performance of on-chip lasers, such as Photonic Crystal Surface Emitting Lasers (PCSEL), and for describing specific optical modes, namely (quasi-) Bound In Continuum (BIC) modes, which can lead to lasing. Theoretically, the *A*- and *B*-modes in an infinite device will not display any surface emission, which is not the case for our finite size of devices. This leads to out-of-plane emission with a finite quality (*Q*) factor. The *E*-mode lacks this anti-symmetry, allowing light to escape the cavity and emit perpendicular to the plane, which enhances emission or reflection for that specific mode and results in lower *Q*. This underscores the importance of understanding how design choices influence their relative wavelength positions within a structure.

Deviations from perpendicular Bragg Diffraction will result in different modes than given above and in the emergence of modes within the structure that possess specific in-plane

wave vector ($k_{||}$) values, forming distinct photonic bands. The magnitude of $k_{||}$ directly influences the emission angle associated with each photonic band and wavelength. By employing FEM, the eigenmodes of the system for specific boundary conditions -- set by choosing a value for $k_{||}$ within the Brillouin zone – can be determined from which photonic bands can be constructed, as shown in Figure 2b. Here, the *x*-axis represents the wave vector path typically moving from the *M*-point, through the *Γ*-point, to the *X*-point within the Brillouin zone, following the path shown in the inset. These points correspond to wave vector values of $(\pi/a, \pi/a)$, *(0,0)* and $(\pi/a, 0)$ respectively, where a is the period. The plot zooms in on approximately 10% of the region toward the *M* and *X* points, as optical modes around *Γ* are the main interest here, as we are looking into surface emission.

The photonic band structure and the field profiles shown apply to devices that extend infinitely. However, in finite and realistically processed devices, this anti-symmetry is disrupted close toward the edges, which allows for upward emission from the *A*- and *B*-modes, albeit at a specific, small angle dependent on the overall size of the structure. In larger structures, this emission intensity diminishes and the emission angle narrows. In contrast, the *E*-mode's emission resembles a Gaussian distribution, where the width is determined by the number of periods in the structure. This results in either a ring-shaped (for *A* or *B*) or Gaussian (for *E*) far field pattern, which can be used experimentally to discern whether the emission originates from the *A/B*-modes or the *E*-mode. Additionally, the polarization of the emitted ring indicates whether the mode is TE or TM. The rings are azimuthally and radially polarized, respectively, and are displayed in Figure 2d. By employing a polarizer, it is possible to differentiate between these two modal polarizations. For TE rings, lobes will appear perpendicular to the polarization axis, whereas for TM they appear parallel.

As previously mentioned, the field distributions in the different materials determine the positions of the modes at *Γ*. This is influenced by both the absolute value of the effective index and the contrast between the refractive indices. Typical values for Cd-based colloidal NC are $n = 1.8 - 2.2$, whereas the SiNx used has $n = 2.0$ in the visible spectrum. The low index contrast $\Delta n \approx 0.2$ between the materials will bring the various optical modes closer together. Due to the low index contrast in colloidal NC/SiNx PhC structures, all six optical modes are typically 30-40 nm spaced apart only. This is in stark contrast with PCSELs made with high index contrast.

Conclusions

In this study, we provided a solid theoretical framework of the light-matter interactions between silicon nitride-based 2D PhC structures and colloidal NCs as light emitting and amplifying medium. In particular, the theory behind the mode congestion feature of low-index contrast systems was explained, displaying challenges to achieve single-moe operation in lasing devices. Whereas several routes can be explored to lift this problem, it must be said that not all laser applications necessitate single-mode operation and that the inherent qualities of the SiNx platform, especially its low loss and wide spectral range, most likely will offset these inherent limitations in future applications.

References

[1] Liu, Junqiu, et al. "High-yield, wafer-scale fabrication of ultralow-loss, dispersion-engineered silicon nitride photonic circuits." *Nature communications* 12.1 (2021): 2236.

[2] Bisschop, Suzanne, et al. "The impact of core/shell sizes on the optical gain characteristics of CdSe/CdS quantum dots." *ACS nano* 12.9 (2018): 9011-9021.

[3] Tanghe, Ivo, et al. "Optical gain and lasing from bulk cadmium sulfide nanocrystals through bandgap renormalization." *Nature Nanotechnology* 18.12 (2023): 1423-1429.

[4] Tanghe, Ivo, et al. "Two-Dimensional Electron–Hole Plasma in Colloidal Quantum Shells Enables Integrated Lasing Continuously Tunable in the Red Spectrum." *ACS nano* (2024).

[5] Ahn, Namyoung, et al. "Optically Excited Lasing in a Cavity-Based, High-Current-Density Quantum Dot Electroluminescent Device." *Advanced Materials* 35.9 (2023): 2206613.

[6] Ahn, Namyoung, et al. "Electrically driven amplified spontaneous emission from colloidal quantum dots." *Nature* 617.7959 (2023): 79-85.

[7] Adachi, Michael M., et al. "Microsecond-sustained lasing from colloidal quantum dot solids." *Nature communications* 6.1 (2015): 8694.

[8] Sakai, Kyosuke, et al. "Lasing band-edge identification for a surface-emitting photonic crystal laser." *IEEE Journal on Selected Areas in Communications* 23.7 (2005): 1335-1340.